Title

Rapid hyperosmotic-induced Ca2+ responses in Arabidopsis thaliana exhibit sensory potentiation and involvement of plastidial KEA transporters

Journal

Proceedings of the National Academy of Sciences of the United States of America, 113(35)

ISSN

0027-8424

Authors

Stephan, Aaron B
Kunz, Hans-Henning
Yang, Eric
et al.

Publication Date

2016-08-30

DOI

10.1073/pnas.1519555113

Peer reviewed

Rapid hyperosmotic-induced Ca^{2+} responses in *Arabidopsis thaliana* exhibit sensory potentiation and involvement of plastidial KEA transporters

Aaron B. Stephan[a], Hans-Henning Kunz[a,b], Eric Yang[a], and Julian I. Schroeder[a,1]

[a]Division of Biological Sciences, Cell and Developmental Biology Section, Food and Fuel for the 21st Century Center, University of California, San Diego, La Jolla, CA 92093; and [b]School of Biological Sciences, Washington State University, Pullman, WA 99164

Contributed by Julian I. Schroeder, July 12, 2016 (sent for review October 2, 2015; reviewed by Elizabeth S. Haswell and Paul E. Verslues)

Plants experience hyperosmotic stress when faced with saline soils and possibly with drought stress, but it is currently unclear how plant roots perceive this stress in an environment of dynamic water availabilities. Hyperosmotic stress induces a rapid rise in intracellular Ca^{2+} concentrations ($[Ca^{2+}]_i$) in plants, and this Ca^{2+} response may reflect the activities of osmo-sensory components. Here, we find in the reference plant *Arabidopsis thaliana* that the rapid hyperosmotic-induced Ca^{2+} response exhibited enhanced response magnitudes after preexposure to an intermediate hyperosmotic stress. We term this phenomenon "osmo-sensory potentiation." The initial sensing and potentiation occurred in intact plants as well as in roots. Having established a quantitative understanding of wild-type responses, we investigated effects of pharmacological inhibitors and candidate channel/transporter mutants. Quintuple mechano-sensitive channels of small conductance-like (MSL) plasma membrane-targeted channel mutants as well as double mid1-complementing activity (MCA) channel mutants did not affect the response. Interestingly, however, double mutations in the plastid K^+ exchange antiporter (KEA) transporters *kea1kea2* and a single mutation that does not visibly affect chloroplast structure, *kea3*, impaired the rapid hyperosmotic-induced Ca^{2+} responses. These mutations did not significantly affect sensory potentiation of the response. These findings suggest that plastids may play an important role in early steps mediating the response to hyperosmotic stimuli. Together, these findings demonstrate that the plant osmo-sensory components necessary to generate rapid osmotic-induced Ca^{2+} responses remain responsive under varying osmolarities, endowing plants with the ability to perceive the dynamic intensities of water limitation imposed by osmotic stress.

osmotic sensing | calcium | salt stress | plastid | abscisic acid

Plants exhibit a wide range of physiological responses to cope with water deprivation by drought and salinity stress (1–3). The properties of biological sensors determine the circumstances and extent to which these coping mechanisms are activated, but the early sensory mechanisms and components regulating the osmotic sensory components in plants are not well understood (see ref. 4 for review). Pioneering studies have demonstrated that *Arabidopsis* seedlings expressing the bioluminescent Ca^{2+} reporter protein aequorin exhibit a rapid rise in intracellular Ca^{2+} ($[Ca^{2+}]_i$) within seconds upon stimulation by NaCl solution (5, 6). This rapid osmotic-induced Ca^{2+} response has been observed in plant species ranging from rice (7) to the basal-branching moss taxon *Physcomitrella patens* (8), indicating that this response may be conserved across the Plantae kingdom. Solutions of either NaCl or iso-osmotic mannitol/sorbitol induce nearly identical rapid Ca^{2+} responses, indicating that the nature of this rapid stimulus is largely osmotic rather than ionic (5, 9, 10). Individual seedling responses tend to be quite heterogeneous, and the response characteristics show variation depending on the accession or extracellular ionic composition (9, 11). It has been demonstrated that, for NaCl stress in particular, Ca^{2+} influx first appears in roots and later in shoots (9), and when roots are stimulated with salt stress, the Ca^{2+} signal propagates to the leaves in waves (12, 13). The root-to-shoot propagation requires the slow vacuolar (SV) channel two-pore calcium channel protein 1 (TPC1), proposed to mediate a Ca^{2+}-induced Ca^{2+} release mechanism (12). However, TPC1 is not required for the rapid osmotic-induced Ca^{2+} response (12). On a longer time scale, Ca^{2+} oscillations have been observed within individual cells (14). Thus, rapid hyperosmotic-induced Ca^{2+} responses represent the initial cytosolic Ca^{2+} rise preceding these secondary Ca^{2+} signaling events that occur throughout the plant.

Given the short time interval between stimulus and response, quantitative interrogation of the rapid hyperosmotic-induced Ca^{2+} response in plants was used as a method to identify a potential osmo-sensory component (15) as well as sensory components for other stimuli such as ATP and rapid alkalization factor (RALF) peptides (16, 17). One mutant line, reduced hyperosmolality-induced $[Ca^{2+}]_i$ increase 1 (*osca1*), was mapped to mutations in a membrane protein At4g04340 (15). Both osca1 and a homolog CSC1 (encoded by the gene At4G22120) were shown to confer osmotically sensitive Ca^{2+}-permeable channel currents (15, 18). It remains unknown, however, how these and other unidentified components of the osmo-sensory components are regulated.

Osmotic stress in plants is dynamic in nature; availability of water to the plant can vary widely depending on soil water capacity, dissolved ionic content, precipitation, atmospheric humidity, temperature, wind speed, and solar irradiance (19). However, it is not known whether a dynamic osmotic environment modulates the activity of the initial osmo-sensory components in plants. Here we present a quantitative study of rapid hyperosmotic-induced Ca^{2+} responses in the plant *Arabidopsis thaliana*. We found that

Significance

How plant roots initially sense osmotic stress in an environment of dynamic water availabilities remains largely unknown. Plants can perceive water limitation imposed by soil salinity or, potentially, by drought in the form of osmotic stress. Rapid osmotic stress-induced intracellular calcium transients provide the opportunity to dissect quantitatively the sensory mechanisms that transmit osmotic stress under environmental and genetic perturbations in plants. We describe a phenomenon whereby prior exposure to osmotic stress increases the sensitivity of the rapid calcium responses to subsequent stress. Further, mutations in plastidial K^+ exchange antiporter (KEA)1/2 and KEA3 transporters were unexpectedly found to reduce the rapid osmotic stress-induced calcium elevation. These findings advance the understanding of the mechanisms underlying the rapid osmotic stress response in plants.

Author contributions: A.B.S., H.-H.K., and J.I.S. designed research; A.B.S. and H.-H.K. performed research; A.B.S. and E.Y. contributed new reagents/analytic tools; A.B.S. and E.Y. analyzed data; and A.B.S. and J.I.S. wrote the paper.

Reviewers: E.S.H., Washington University in Saint Louis; and P.E.V., Academia Sinica.

The authors declare no conflict of interest.

[1]To whom correspondence should be addressed. Email: jischroeder@ucsd.edu.

This article contains supporting information online at www.pnas.org/lookup/suppl/doi:10.1073/pnas.1519555113/-/DCSupplemental.

seedlings preexposed to mild osmotic stress exhibited larger, more robust rapid Ca^{2+} responses to subsequent hyperosmotic stress. We term this response "osmo-sensory potentiation."

Ca^{2+} is not only released across the plasma membrane from the apoplast; several organelle types may act as $[Ca^{2+}]_i$ storage pools (20, 21). We further investigated several candidate mutant genes and found that members of the plastidial K^+ exchange antiporter (KEA) transporter family are necessary for eliciting wild-type levels of rapid hyperosmotic-induced Ca^{2+}, but *kea* mutant lines were still largely capable of exhibiting sensory potentiation. Together, these results demonstrate that the sensitivities of the osmo-sensory components are capable of being tuned according to previous stimulation and indicate an important role for plastidial ion transporters in stress-induced $[Ca^{2+}]_i$ elevation.

Results

Features of Rapid Hyperosmotic-Induced Ca^{2+} Responses. Wild-type *Arabidopsis* seedlings of the ecotype Col-0 expressing aequorin under the control of the strong and constitutive 35S promoter (henceforth referred to as "wild-type Col-0") were grown for 1 wk in individual wells of 96-well plates. The seedlings were pretreated with the cofactor coelenterazine to reconstitute the active aequorin Ca^{2+} reporter complex. Stimulation solutions were applied automatically to each well while Ca^{2+}-dependent light emission from individual seedlings was measured. We observed that stimulation of the seedlings by hyperosmotic stress resulted in a rapid, transient rise in $[Ca^{2+}]_i$ (Fig. 1 *A–D*), consistent with previous reports (5, 9, 12, 15). When seedlings were stimulated by a low-osmolarity solution iso-osmotic to the existing medium, only small responses were observed (Fig. 1 *A* and *B*). These small responses could be the result of the seedlings sensing a mechanical force caused during application of the stimulus into the wells containing the seedlings (22, 23). We found that these "mechano-sensory" responses peaked consistently within 2 s and returned to baseline by 20 s under the imposed conditions (Fig. 1 *A* and *B*). As the osmolarities of the stimuli were increased, the amplitudes of the rapid Ca^{2+} responses increased dramatically (Fig. 1 *A–D*). These osmo-sensory responses varied from seedling to seedling in terms of amplitudes and kinetics (Fig. 1 *C* and *D*), as has been noted previously (9). However, we observed that nearly all hyperosmotic-induced Ca^{2+} responses exhibited an initial peak in free cytosolic Ca^{2+} within 5 s of stress application and exhibited an additional peak or several secondary peaks that were much more variable in amplitude and kinetics (Fig. 1 *C* and *D*). Occasionally the secondary peaks blended in with the first peak, giving the impression of a single, larger peak (e.g., black trace in Fig. 1*C*) (24). The variation in amplitude is not caused by variation in aequorin expression levels, because relative Ca^{2+} concentrations were calculated based on calibrated normalization to total active aequorin protein in each seedling (*Materials and Methods*) (25). Indeed, independent aequorin-transformant wild-type Col-0 lines varying by more than fivefold in aequorin expression levels showed indistinguishable mean hyperosmotic-induced Ca^{2+} responses after normalization (Fig. S1). Because of the inherent variability from seedling to seedling, we developed an analysis program that quantifies more than 40 features of individual seedling responses including primary and secondary peak amplitudes, time to peaks, decay rates, integrated areas under the peaks, and principal components, and automated plots measured features for individual seedlings as well as averages of replicate seedlings for any tested treatment or genotype (*Materials and Methods*).

To determine how a dynamic osmotic environment affects hyperosmotic-induced Ca^{2+} responses, we first established how different response parameters varied as a function of stimulus osmolarity. As the log(osmolarity) of the stimulus increased, primary peaks rose in a quasisigmoidal fashion (Fig. 1*E*). The EC_{50}, determined by the osmolarity needed to elicit 50% of the maximal response, was ~316 mOsmol/L for primary peak amplitudes. The

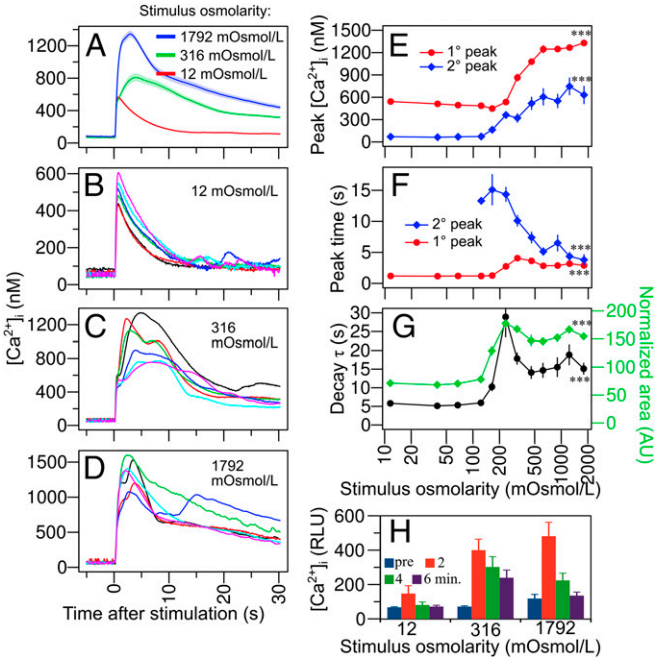

Fig. 1. Osmotic dose dependency of rapid Ca^{2+} response parameters. (*A*) Average $[Ca^{2+}]_i$ responses (solid lines) ± SEM (transparent shading) of 39–40 seedlings stimulated with an application of NaCl solutions resulting in an osmolarity of 12 (red), 316 (green), or 1,792 (blue) mOsmol/L at time = 0. (*B–D*) Six representative individual seedling Ca^{2+} responses to selected solution osmolarities. Note the differing *y* axis scales in *B–D*. (*E–G*) Influence of stimulus osmolarity on measured parameters of the Ca^{2+} response, including primary (1°) and secondary (2°) peak amplitudes (*E*), time from stimulation to the peaks (*F*), and response termination kinetics as quantified by the decay constant τ (black trace) and the area under the normalized response curve (green trace) (*G*). n = 31–40 seedlings per data point in *E–G*. Statistical comparisons were made between the lowest and highest stimulus concentrations using one-way ANOVA with the Tukey honestly significant difference (HSD) post hoc test. ***$P < 0.001$. (*H*) Baseline Ca^{2+} concentrations immediately preceding (pre) and 2, 4, and 6 min following stimulation with NaCl solutions to result in the indicated osmolarity. Error bars represent ± SEM.

time from stimulation to primary peak increased slightly but significantly (Fig. 1*F*); the time from stimulation to the largest secondary peaks was reduced dramatically at higher osmolarities (Fig. 1*F*). Termination kinetics, measured in terms of an exponential decay constant (τ) and integrated area under normalized curves showed that termination rates slowed as the hyperosmotic stimulus was increased but then fell slightly at very high stimulus intensities (Fig. 1*G*). The sensory threshold, determined by the osmolarity that achieves above-background responses, was determined to be in the range of 123–164 mOsmol/L for the parameters measured here (Fig. 1 *E–G*).

Under the stimulation paradigm used in this study, the hyperosmotic stress is applied to a well containing the seedling, so the stress remains constant after application of the stress. However, the $[Ca^{2+}]_i$ levels did not remain at peak elevations. Instead, the Ca^{2+} levels decayed dramatically within 30 s after stimulation (Fig. 1 *A–D*) and approached prestimulus levels several minutes after stimulation for low-intensity (12 mOsmol/L) and high-intensity (1,792 mOsmol/L) stimuli (Fig. 1*H*). The intermediate-intensity (316 mOsmol/L) stimulus showed a slower decay time course (Fig. 1 *G* and *H*).

Potentiation of Rapid Hyperosmotic Stress-Induced Ca^{2+} Responses by Prior Hyperosmotic Exposure. We next preexposed *Arabidopsis* seedlings to intermediate levels of hyperosmotic stress for prolonged durations (~1–3 h) and measured rapid Ca^{2+} responses to

subsequent hyperosmotic stimuli. Interestingly, we found that raising the prestimulus osmolarity from 21 mOsmol/L to 149 mOsmol/L resulted in larger, more robust hyperosmotic-induced Ca^{2+} responses (Fig. 2*A*). By quantifying the features of hyperosmotic responses as a function of starting osmolarity, we found that the amplitude of the primary peak, but not the amplitude of the secondary peak, was increased by the starting osmolarity (Fig. 2*B* and Fig. S2 *C* and *D*). Because increasing background stress resulted in larger response amplitudes, we term this phenomenon "osmo-sensory potentiation," after analogous potentiation phenomena described in neuroscience (26) and pharmacology (27). Osmo-sensory potentiation was confirmed to occur in two independent aequorin-expressing lines (*Materials and Methods*). When the background stress was raised above ∼212 mOsmol/L, the primary peak amplitudes were no longer amplified but instead returned to nonpotentiated levels (Fig. 2*B*). Sensory potentiation of hyperosmotic-induced Ca^{2+} responses occurred consistently, regardless of whether the osmolyte was sorbitol or NaCl in either the preexposure medium or the stimulation solution (Fig. S2 *A* and *B*).

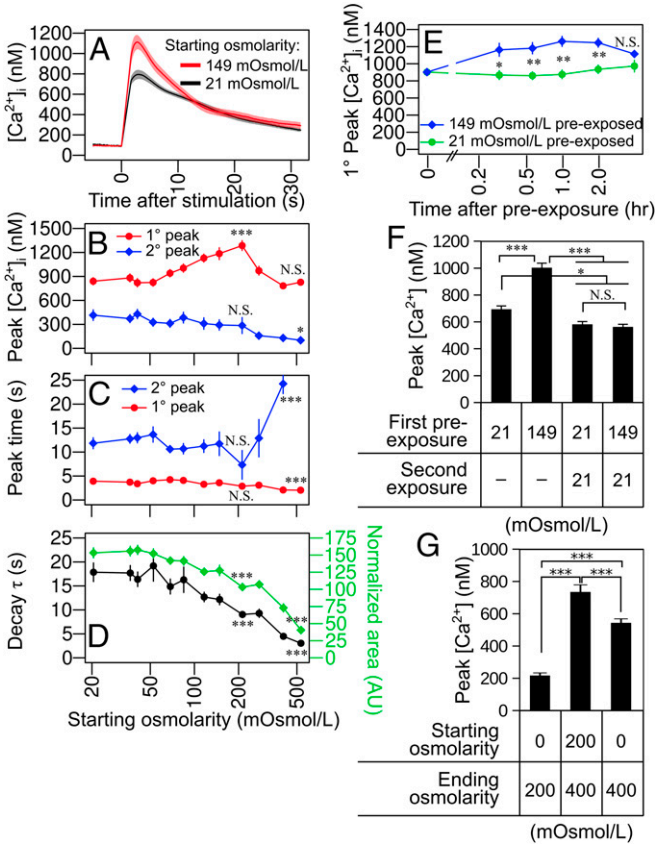

Fig. 2. Potentiation of rapid hyperosmotic-induced Ca^{2+} responses by prior exposure of seedlings to hyperosmotic stress. (*A*) Average Ca^{2+} responses (solid lines) ± SEM (transparent shading) of seedlings preexposed for 1–2 h to low-osmolarity (21 mOsmol/L, black trace) and high-osmolarity (149 mOsmol/L, red trace) medium, stimulated with an injection of 0.7 volumes of 700-mM sorbitol solution at time = 0. n = 40 seedlings per trace. (*B–D*) Influence of starting osmolarity before stimulation on measured parameters of the Ca^{2+} response, including primary and secondary peak amplitudes (*B*), time from stimulation to the peaks (*C*), and response termination kinetics as quantified by the decay constant τ (black trace) and the area under the normalized response curve (green trace) (*D*). n = 40 seedlings per data point in *B–D*. Statistical comparisons were made between an indicated data point and the lowest starting osmolarity data point using one-way ANOVA with the Tukey HSD post hoc test. (*E*) Time course of sensory potentiation, comparing primary peak amplitudes of seedlings stimulated with an application of hyperosmotic medium and preexposed to low-osmolarity (21 mOsmol/L; green trace) or high-osmolarity (149 mOsmol/L; blue trace) medium as a function of time from preexposure to time of stimulation. n = 62–69 seedlings per data point. Statistical comparisons were made between preexposure to 21 mOsmol/L and preexposure to 149 mOsmol/L at each time point using one-way ANOVA with the Tukey HSD post hoc test. (*F*) Reversibility of sensory potentiation assessed by serial exposure to either low-osmolarity (21 mOsmol/L) or high-osmolarity (149 mOsmol/L) medium. n = 91–93 seedlings per data point. (*G*) Ca^{2+} responses were recorded in the presence of starting osmolarities of 0 or 200 mOsmol/L and ending osmolarities of 200 or 400 mOsmol/L imposed by sorbitol stress. n = 46–58 seedlings per condition. Error bars represent ± SEM. Statistical comparisons were made between conditions using one-way ANOVA with the Tukey HSD post hoc test. *P < 0.05; **P < 0.01; ***P < 0.001; N.S., P > 0.05.

Preexposure to higher levels of hyperosmotic stress (512 mOsmol/L) resulted in a modest shortening of the time required to reach the primary Ca^{2+} peak (Fig. 2*C*). In contrast, the time required to reach the secondary peak was lengthened significantly at high starting osmolarities (Fig. 2*C*). Preexposure to higher levels of hyperosmotic stress also resulted in more rapid termination kinetics and reduced area under the normalized peaks (Fig. 2*D*).

Time-course analysis revealed that sensory potentiation began to occur within 18 min after preexposure to intermediate osmolarity and that the sensory potentiation peaked by 2 h after preexposure (Fig. 2*E*). To determine whether this sensory potentiation was reversible, we reexposed the seedlings to low-osmolarity medium a second time before high-osmolarity stimulation and Ca^{2+} measurement. We found the potentiation effects of the first preexposure to high-osmolarity medium could be erased completely by subsequent exposure to low-osmolarity medium before hyperosmotic stimulation (Fig. 2*F*).

To test further how potentiation is affected by both relative and final osmolarity changes, we varied the starting (pretreatment) and ending (stimulus) osmolarities and measured the resulting Ca^{2+} responses. We found that the solutions starting from 200 and ending at 400 mOsmol/L elicited a larger Ca^{2+} response than the solutions starting from 0 and ending at 200 mOsmol/L and those starting from 0 and ending at 400 mOsmol/L (Fig. 2*G*). These results demonstrate that elevating the starting osmolarity potentiates the subsequent Ca^{2+} in response to the same ending osmolarity and that the plant may sense relative changes in stimulus intensity rather than total or final osmolarity.

Osmo-Sensing and Hyperosmotic-Induced Sensory Potentiation Occur in Roots. There is some debate about the site of initial generation of rapid hyperosmotic-induced Ca^{2+} responses, and the site may depend on experimental conditions. Although some studies show that the Ca^{2+} signal first appears in roots (9, 12), another indicates that the Ca^{2+} signal may occur simultaneously and more strongly in the shoots (15). The Ca^{2+} response occurs in many cell types, but it is reported to be largest and to occur earliest within cells of the root epidermis (24, 28). We measured hyperosmotic-induced Ca^{2+} responses in isolated roots, isolated shoots, and whole seedlings (Fig. 3 *A* and *B*). The hyperosmotic-induced Ca^{2+} response was larger in roots than in shoots when both were exposed to the same stimulus (Fig. 3*B*). By varying the starting osmolarity, we determined that whole seedlings and isolated roots were competent to exhibit potentiation at a 90% confidence level, but isolated shoots were not (Fig. 3*B*).

To analyze the spatial distribution of Ca^{2+} dynamics more directly in whole, intact seedlings, plants were stimulated uniformly with hyperosmotic stress and were imaged with a CCD camera (Fig. 3*C*). Rapid luminescence from the aequorin reporter was emitted almost exclusively from the roots, most strongly in the zones close to the root tip, 0–30 s after stimulation (Fig. 3*C*). A lack of light emission from the leaves could not be explained by the absence of aequorin reporter in the leaves, because subsequent discharge of total remaining aequorin with 2 M $CaCl_2$ + 20% (vol/vol) ethanol revealed an abundance of active aequorin reporter remaining in leaves (Fig. 3*D*).

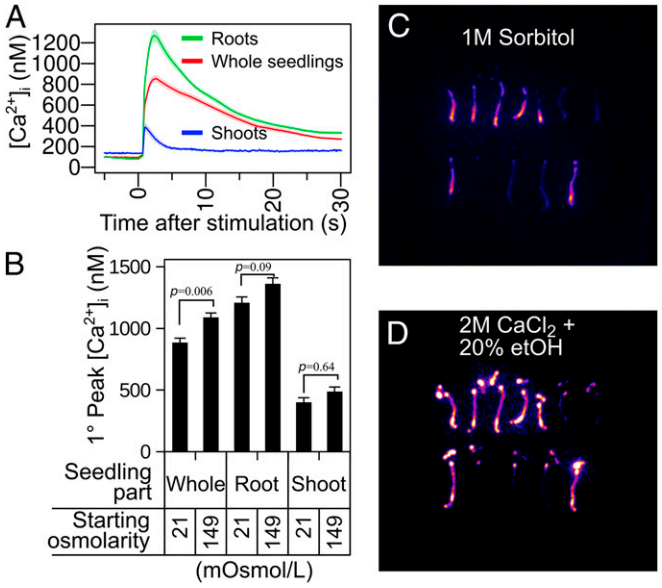

Fig. 3. Rapid hyperosmotic-induced Ca^{2+} responses and potentiation occur primarily in roots. (*A*) Average Ca^{2+} responses (solid lines) ± SEM (transparent shading) of 1-wk-old whole seedlings (red trace), isolated roots (green trace), and isolated shoots (blue trace) preexposed for 1–2 h to low-osmolarity (21 mOsmol/L) medium and stimulated with an application of hyperosmotic sorbitol solution at time = 0. n = 37–40 seedlings per trace. (*B*) Primary peak amplitudes whole seedlings, isolated roots, and isolated shoots stimulated with an application of hyperosmotic medium and preexposed to low-osmolarity (21 mOsmol/L) or moderate-osmolarity (149 mOsmol/L) medium. Error bars represent ± SEM. Statistical comparisons were made between starting osmolarity conditions using one-way ANOVA with the Tukey HSD post hoc test. *P* values are indicated. (*C* and *D*) Pseudocolored photographs depicting light emission of intact whole seedlings in response to hyperosmotic shock (1 M sorbitol, signal integrated for 30 s) (*C*) and subsequently to 2 M $CaCl_2$ + 20% ethanol, which discharges all remaining aequorin (signal integrated for 1 min) (*D*).

Additive Effects of Abscisic Acid Signaling and Hyperosmotic-Induced Potentiation. One possible mechanism for sensory potentiation could involve positive feedback from downstream hyperosmotic-induced signaling components on the upstream osmo-sensory components. Because osmotic stress induces abscisic acid (ABA) biosynthesis (29, 30), and ABA enacts a multitude of physiological changes including modulation of ion channel activity and transcriptional reprogramming (31), we tested the effects of exogenous ABA application on hyperosmotic-induced Ca^{2+} responses. In 6 of 12 experiments, preexposure of seedlings to ABA resulted in larger-amplitude hyperosmotic-induced Ca^{2+} responses (Fig. 4 *A*–*C*). In the other six experiments, no effect of adding exogenous ABA was observed. In experiments in which ABA resulted in larger-amplitude hyperosmotic-induced Ca^{2+} responses, 2 μM ABA was sufficient to reach saturation, and 10 μM ABA did not further increase the response amplitudes (Fig. 4 *A* and *B*). To determine whether this ABA effect may interact with the potentiation of the response by elevated starting osmolarity, we preexposed seedlings to either low- or moderate-hyperosmolarity medium that either lacked or contained ABA. We found that the increases in amplitude induced by either ABA preexposure or hyperosmotic preexposure alone were additive when the seedlings were preexposed to both ABA and medium with high starting osmolarity (Fig. 4*C*); two-way ANOVA (32) analysis indicated that preexposure to ABA together with preexposure to a starting osmolarity preexposure significantly increased the primary peak amplitudes ($P = 2.3 \times 10^{-4}$ and $P = 6.79 \times 10^{-8}$, respectively), but there was no detectable interaction between the ABA and starting osmolarity pretreatments ($P = 0.89$). This result suggests that potentiation of the hyperosmotic-induced Ca^{2+} response by preexposure to hyperosmotic stress occurs by mechanisms that are at least partially distinct from those involved in ABA signaling.

To address this question further, we made use of a recently developed ABA-signaling antagonist, hexasulfanyl-ABA (HS-ABA). This ABA analog has been shown to bind the PYR/PYL family of ABA receptors and to disrupt the receptor interactions with inhibitory PP2C proteins, thereby leading to constitutive repression of ABA signaling (33). HS-ABA drastically reduced the amplitudes of the hyperosmotic-induced Ca^{2+} responses, eliminating any discernible effect of hyperosmotic pretreatment potentiation (Fig. 4*D*). Two-way ANOVA demonstrated that starting osmolarity and HS-ABA treatment had large effects on primary peak amplitudes ($P = 1.8 \times 10^{-4}$ and $P < 2 \times 10^{-16}$, respectively). Nevertheless, no significant interaction was found between HS-ABA treatment and starting osmolarity (i.e., the treatments appeared to be additive) ($P = 0.07$). If the effects of HS-ABA

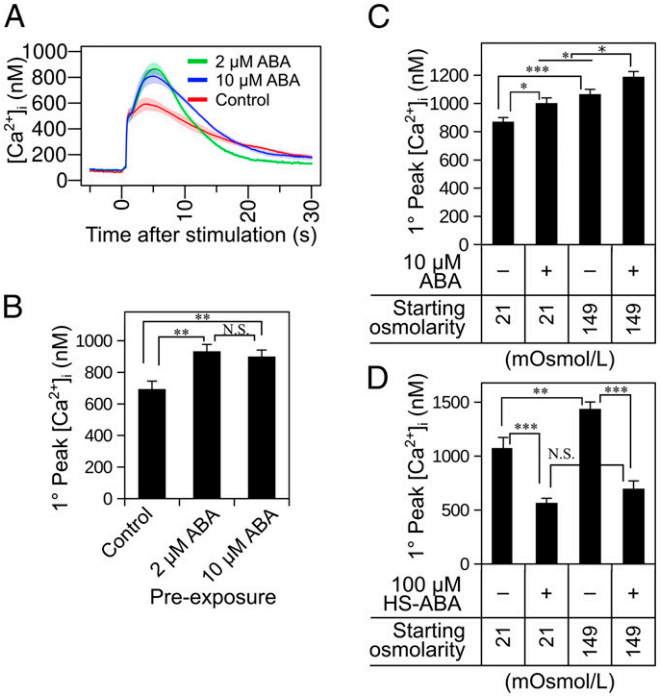

Fig. 4. Influence of ABA on Ca^{2+} response amplitudes and potentiation. (*A*) Average Ca^{2+} responses (solid lines) ± SEM (transparent shading) of 1-wk-old whole seedlings preexposed for 1–2 h to low-osmolarity (21 mOsmol/L) medium with or without ABA at the indicated concentrations and stimulated with an application of hyperosmotic sorbitol solution at time = 0. n = 20–23 seedlings per trace. (*B*) Quantification of primary peak amplitudes in *A*. Statistical comparisons were made between conditions using one-way ANOVA with the Tukey HSD post hoc test. $^{**}P < 0.01$; N.S., $P > 0.05$. (*C*) Additive effects of preexposure to ABA and elevated osmolarity on Ca^{2+} responses in seedlings stimulated with an application of hyperosmotic medium. n = 47–48 seedlings per data point. Two-way ANOVA analysis revealed that ABA preexposure and starting osmolarity preexposure significantly increased the primary peak amplitudes ($P = 2.3 \times 10^{-4}$ and $P = 6.79 \times 10^{-8}$, respectively), but there was no detectable interaction between the treatments ($P = 0.89$). *P* values were calculated by the Tukey HSD post hoc test. $^{*}P < 0.05$; $^{***}P < 0.001$. (*D*) Effects of the ABA antagonist HS-ABA (100 μM) on hyperosmotic-induced Ca^{2+} response amplitudes in seedlings preexposed to low- or high-osmolarity medium. n = 30–32 seedlings per data point. Error bars represent ± SEM. Two-way ANOVA revealed that starting osmolarity and HS-ABA treatment had large effects on primary peak amplitudes ($P = 1.8 \times 10^{-4}$ and $P < 2 \times 10^{-16}$, respectively). No significant interaction was seen between HS-ABA treatment and starting osmolarity. Depicted *P* values were calculated by the Tukey HSD post hoc test. $^{*}P < 0.05$; $^{**}P < 0.01$; $^{***}P < 0.001$; N.S., not significant. The influence of ABA on the Ca^{2+} response amplitudes was observed in 6 of 12 experiments. *A* and *B* show one experiment, and *C* shows another experiment.

indeed result from specific inhibition of ABA signaling, this result could indicate that a certain level of basal ABA signaling is a prerequisite for maintaining the responsiveness of the osmo-sensory components, regardless of potentiation status.

Survey of Ion Transporters That May Play a Role in Eliciting Hyperosmotic-Induced Ca^{2+} Responses. Only one mutant, OSCA1, has been described to date that impairs the rapid osmotic stress-induced Ca^{2+} elevation (15). Previous studies suggest that the Ca^{2+} stores responsible for rapid hyperosmotic-induced Ca^{2+} influx may include both the apoplast and intracellular organelles, because the extracellular Ca^{2+}-signaling inhibitors La^{3+}, Gd^{3+}, and EGTA and several $[Ca^{2+}]_i$-signaling inhibitors all affect the amplitude and kinetics of the osmotic-induced Ca^{2+} response (5, 9). We tested a variety of pharmacological agents and found that $LaCl_3$, $GdCl_3$, amiloride, and D-*cis*-diltiazem dampened the rapid osmotic-induced Ca^{2+} response (Fig. S3 and Table S1), but DNQX, CNQX, D-AP5, verapamil, tetracaine, Ruthenium red, U-73122, H-8, Methylene blue, NS-2028, and ODQ did not dampen the rapid osmotic-induced Ca^{2+} response (for details, see Table S1).

We assessed candidate mutant lines for altered hyperosmotic-induced Ca^{2+} responses, including mechano-sensitive plasma membrane-localized channels. No significant effects were observed in the higher-order mechanosensitive Ca^{2+} channel root *Mid1-complementing activity mca1;mca2* (AT4G35920, AT2G17780) double mutant (34, 35) or the plasma membrane-targeted members of the mechano-sensitive channel of small conductance (*MscS*)-like family *msl4,5,6,9,10* (AT1G53470, AT3G14810, AT1G78610, AT5G19520, AT5G12080) quintuple mutant (Fig. S4) (36). Additionally, it has been shown previously that the *tpc1* (AT4G03560) mutants in the vacuolar Ca^{2+}-activated Ca^{2+}-permeable SV channel do not affect the rapid osmotically induced increase in Ca^{2+} but rather impair the ensuing root-to-shoot Ca^{2+} wave (12).

It has recently become evident that plastids represent a significant pool for Ca^{2+} release in plants (21, 37, 38). We measured hyperosmotic-induced Ca^{2+} responses in plastidial-localized *kea* mutant lines. KEA1 (AT1G01790) and KEA2 (AT4G00630) are targeted to the inner plastid envelope membrane and are required for plastid ion homeostasis and osmo-regulation (39–41). Loss of function results in morphologically swollen plastids and decreased photosynthetic activity (41). Because KEA1 and KEA2 act as K^+/H^+ antiporters, mutation of these genes is expected to perturb the electrochemical potential of these—and possibly other—ions across the envelope membrane. We found that *kea1-2kea2-2* double mutants displayed a substantially reduced amplitude of the rapid hyperosmotic-induced Ca^{2+} response at high starting osmolarity (Fig. 5 *A* and *B*). Comparing conditions of low and high starting osmolarity, we found that the *kea1-2kea2-2* double mutant line was competent to exhibit sensory potentiation despite overall reduced amplitudes compared with wild type (Fig. 5 *A* and *B*). Transgenic expression of wild-type *KEA2* under the control of the AtUBQ10 promoter was sufficient to rescue the low-amplitude Ca^{2+} phenotype of the *kea1-2kea2-2* double mutant (Fig. 5 *E* and *F*).

We next tested a mutant in the *KEA3* (AT4G04850) gene; KEA3 is localized to the thylakoid membrane (41, 42). Ca^{2+} storage occurs within the plastid lumen. *Kea3* mutants show morphologically intact chloroplasts, but mutation results in altered absorption of photosynthetic energy under dynamic light conditions (42). Interestingly, we found that the *kea3-1* mutant line displayed a reduced amplitude of the hyperosmotic-induced Ca^{2+} response, much like the *kea1-2kea2-2* double-mutant line (Fig. 5 *C* and *D*), and likewise was still competent to exhibit sensory potentiation (Fig. 5 *C* and *D*). Thus, the impairment in osmotic stress-induced Ca^{2+} cannot be linked solely to the aberrant chloroplast morphology of the *kea1-kea2* mutant (41) but correlates with the effects of both mutants on chloroplast ion homeostasis and photosynthetic efficiency.

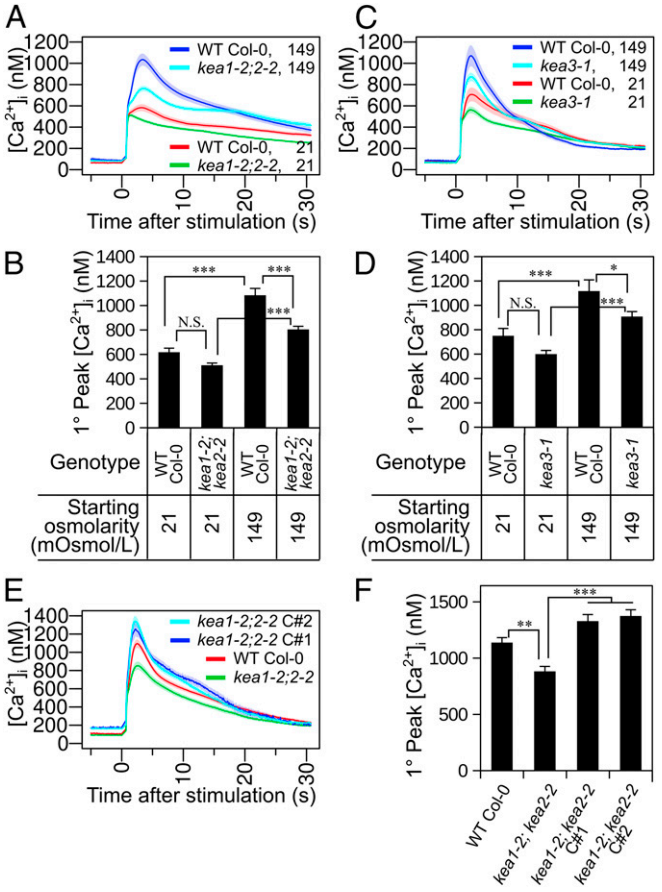

Fig. 5. Plastidial *kea* mutations reduce rapid hyperosmotic-induced Ca^{2+} response amplitudes but do not eliminate sensory potentiation. (*A*) Average Ca^{2+} responses (solid lines) ± SEM (transparent shading) of 1-wk-old wild-type (Col-0) or *kea1-2; kea2-2* double mutant seedlings preexposed for 1–2 h to low-osmolarity (21 mOsmol/L) or high-osmolarity (149 mOsmol/L) medium and stimulated with an application of hyperosmotic sorbitol solution at time = 0. n = 44–64 seedlings per trace. (*B*) Quantification of primary peak amplitudes in *A*. Two-way ANOVA demonstrated that the effects of both genotype and starting osmolarity on primary peak amplitudes were highly significant ($P = 2.77 \times 10^{-7}$ and 2.0×10^{-17}, respectively) and that the interaction between genotype and starting osmolarity was also significant ($P = 0.01$). Statistical comparisons were made with the Tukey HSD post hoc test. (*C*) Average Ca^{2+} responses (solid lines) ± SEM (transparent shading) of 1-wk-old wild-type (Col-0) or *kea3-1* mutant seedlings preexposed for 1–2 h to low-osmolarity (21 mOsmol/L) or high-osmolarity (149 mOsmol/L) medium and stimulated with an application of hyperosmotic sorbitol solution at time = 0. n = 28–66 seedlings per trace. (*D*) Quantification of primary peak amplitudes in *C*. Two-way ANOVA demonstrated that the effects of both genotype and starting osmolarity on primary peak amplitudes were significant ($P = 4.5 \times 10^{-4}$ and 6.69×10^{-10}, respectively), but the interaction between genotype and starting osmolarity was not significant (P = 0.59). Statistical comparisons were made with the Tukey HSD post hoc test. (*E* and *F*) Genetic complementation with a wild-type copy of *Kea2* can rescue the reduced amplitude phenotype of the *kea1-2;kea2-2* double mutant. C#1 and C#2 represent independent complementation lines. Error bars represent ± SEM. Statistical comparisons were made using one-way ANOVA with the Tukey HSD post hoc test. *$P < 0.05$; **$P < 0.01$; ***$P < 0.001$; N.S., $P > 0.05$.

Discussion

Here we report that early sensory components leading to rapid osmotic-induced Ca^{2+} responses in plants can be up-regulated ("potentiated") by prior exposure to osmotic stress, whereas mutation of plastidial KEA transporters results in reduced rapid Ca^{2+} elevation. Because plants exhibit rapid hyperosmotic-induced Ca^{2+} responses with or without preexposure to osmotic stress, this finding indicates that the sensory components are always present

and functional. However, the expression, activity, or sensitivity of the sensory components is increased after a previous experience of hyperosmotic stress, thereby exhibiting sensory potentiation. Important and interesting examples in the literature describe the enhancement of responses after experiencing stress, sometimes referred to as "priming" or "memory" (43–46). The present study, however, reports that the earliest sensory components of the rapid osmotic stress response can be up-regulated in such a manner. Sensory potentiation, as described here, is distinct from these previously described examples because all responses downstream of the initial perception event could be affected. Moreover, the rapid onset and reversibility of sensory potentiation suggest that this phenomenon may be of key importance for "on-the-fly" adjustment of the sensitivity to osmotic conditions as experienced by plant roots in soils when experiencing osmotic stress.

We found that under constant hyperosmotic stimulation, the Ca^{2+} response returns to baseline. This return to baseline suggests that negative feedback mechanisms must exist to inactivate sensory components, including closing Ca^{2+} channels and removing cytosolic Ca^{2+} by active transport (47). Many sensory systems exhibit a similar return to baseline, which is termed "sensory adaptation" (48); examples include mammalian vision and audition, bacterial chemotaxis, and yeast osmoregulation. These systems require integral feedback control to balance sensory components' activation with inactivation (49, 50). Returning to baseline ensures that the system remains responsive to further relative changes in stimulus intensity. Together, these data indicate that the plant may sense relative changes in stimulus intensity rather than total or final osmolarity.

Although we had hypothesized initially that ABA elevation induced by osmotic stress could feed back to up-regulate the osmosensory components, we found that the increase in sensitivity caused by ABA is more variable than and is largely independent of the increase in sensitivity caused by prior exposure to hyperosmotic stress (Fig. 4). Despite our best efforts to control environmental conditions, the effects of exogenous ABA application varied from experiment to experiment. Given that ABA had an effect in only half of our tested experiments and that HS-ABA could reduce the amplitude of osmotic-induced Ca^{2+} responses, we hypothesize that a basal amount of ABA is required for osmotic-induced Ca^{2+} responses and that, once that basal level is reached, additional ABA-dependent potentiation may be limited. This hypothesis can be tested further in the future with mutant lines that are deficient in ABA biosynthesis. We observed a rapid (<20-min) onset of potentiation by preexposure to hyperosmotic stress (Fig. 2*E*), but it has been observed that osmotic-induced ABA increases in roots occur on a substantially slower timescale (51). Therefore, it is unlikely that a rapid increase in ABA concentration can account for osmotic-induced potentiation.

The finding that hyperosmotic stress results in an increase in $[Ca^{2+}]_i$ raises the question of which Ca^{2+} stores are important for this response. Our analyses of the *mca1;mca2* double mutant and the *msl* quintuple mutant show that other channels are required to display the rapid wild-type osmotic-induced Ca^{2+} responses. Our analyses of the plastidial KEA transporters offer initial insight into this question. KEA1 and KEA2 are localized to the inner envelope of the plastid, whereas KEA3 is localized to the thylakoid membrane (39, 41, 42). Although *kea1-2kea2-2* double mutants display phenotypes associated with severely impaired chloroplast functions (41), the *kea3-1* mutant line does not affect chloroplast morphology and is known to display electron transport phenotypes under dynamic light situations (42). In this study we found that both *kea1-2kea2-2* double mutants and *kea3-1* mutants showed reduced osmotic-induced Ca^{2+} responses despite being grown in standard lighting conditions. These results offer the tantalizing prospect that plastidial membrane energetics and Ca^{2+} stores may be linked and required for wild-type hyperosmotic-induced Ca^{2+} responses (21, 52). In animal systems, for instance, it has been demonstrated that mitochondria play an important function in Ca^{2+} release (53, 54). A recent study shows that *KEA1*, *KEA2*, and *KEA3* transcripts are detectable in roots (55). Additionally, root leucoplasts have intracellular membranous lamellar vesicles and plastoglobules (56), the latter of which has significant association with thylakoids in terms of proteome composition (57). Indeed, a recent publication demonstrates the existence of root plastid calcium signaling in response to various chemical stimuli (58). Thus, the calcium signaling phenotype found in the *kea* mutants may be attributable to disrupted root plastid ion homeostasis, but presently an indirect effect (leaf-to-root) or systemic effect cannot be excluded and will require further analyses. The effects of these mutations could be more indirect, affecting ion homeostasis or osmotic perception at the cell surface or in other organelles. Note that mutations in the kea3 transporter do not visually affect chloroplast ultrastructures (41, 42). It has been reported that disrupted plastid osmoregulation in the *msl2msl3* double mutant activates drought-related phenotypes in the absence of an external stress (59). The present study highlights that the involvement of plant plastids in the initial osmotic sensory events deserves further attention.

A novel family of osmotically gated Ca^{2+}-permeable ion channels has been reported in plants (15, 18), and mutations of one family member are the only mutations known to reduce hyperosmotic-induced Ca^{2+} responses primarily in leaves (15). Our study identifies the regulation of the osmo-sensory components by preceding exposure to hyperosmotic stress (potentiation), by the hormone ABA, and by the activities of plastid-localized KEA transporters. These results suggest that the initial osmotic perception events leading to induction of rapid $[Ca^{2+}]_i$ elevations represent a complex trait that is influenced by several factors. Taken together, the results in this work will guide mechanistic studies toward elucidating the osmosensory components in plants.

Materials and Methods

***Arabidopsis* Plant Lines.** Wild-type Col-0 *Arabidopsis* seedlings harboring a transfer DNA (T-DNA) insertion carrying a 35S:Apoaequorin expression cassette were used throughout this study. The lines were either direct descendants of the original kanamycin-resistant pMAQ2 line (60) (shared by Marc Knight, Durham University, Durham, UK and Zhen-Ming Pei, Duke University, Durham, NC) or an independently generated hygromycin-resistant line (shared by Antony Dodd, Bristol University, Bristol, UK). Both lines showed nearly identical expression levels of Apoaequorin, and sensory potentiation was confirmed to occur in both lines. The hygromycin-resistant 35:Apoaequorin line was crossed to the *kea1-2;2-2* (SAIL_1156_H07; SALK_020285) double-mutant and the *kea3-1* (SAIL_556_E12) single-mutant lines (41). The resulting F1 individuals were self-pollinated, and F2 progeny were genotyped and assayed for aequorin expression (41). The F2 individuals that were homozygous for the intended *kea* mutations as well as expressing aequorin were propagated to the F3 generation and tested for hyperosmotic-induced Ca^{2+} responses. Four F3 lines were tested with similar results. *Mca1;2* mutants, provided by Hidetoshi Iida, Okazaki Institute for Integrative Bioscience, National Institutes of Natural Sciences, Okazaki, Aichi, Japan, and *Msl4;5;6;9;10* mutants, provided by Elizabeth Haswell, Washington University in St. Louis, St. Louis, were transformed by the agrobacterium-mediated floral-dip method using a pMAQ2-NEW vector provided by Zhen-Ming Pei, Duke University. T1 transformants were selected based on Basta resistance and aequorin expression. Two T2 lines were tested for each mutant combination. For the *Kea* complementation experiment, the *kea1-2;kea2-2* double mutant expressing aequorin was transformed by the agrobacterium-mediated floral-dip method using a vector expressing Kea2-mVenus fusion protein under the control of the UB10 promoter (41). T1 transformants were selected based on enhanced hygromycin resistance and nonchlorotic leaves, indicating functional complementation. Two T2 lines were tested for osmotic-induced Ca^{2+} responses by analyzing the rescued *kea*-expressing lines (approximately three of four lines), as determined by wild-type green leaf appearance.

Luminometry Measurements of Ca^{2+} Responses in Seedlings. Ethanol-sterilized seeds were plated individually in wells of sterile, white, 96-well microplates (BD Biosciences) containing 130 μL of medium composed of 1/2 Murashige and Skoog (MS) medium (2.2 g/L), 0.5 g/L MES, 1% sucrose, and 0.08% Phyto Agar (Phytotek). The low percentage of Phyto Agar provided modest support for seedling growth while allowing subsequent rapid mixing of injected pretreatment solutions and stimulus solutions. The clear lids were sealed with Parafilm

(Bemis NA) to prevent medium evaporation. The seedlings were cold stratified for 2–3 d at 4 °C in the dark and then were grown for 6.5 d in a growth cabinet (16-h light/8-h dark, 22 °C, 60–80 μEm^2/s light intensity). Twelve to fourteen hours before the experiment, 130 μL of water containing 2 μM native coelenterazine (Ctz) (Promega) was added to each well. The lid was replaced on the plate but was not sealed with Parafilm again. The plate was covered by aluminum foil to prevent light-induced degradation of Ctz and was incubated overnight in the growth cabinet.

The following day, just before experiments, 130 μL of medium was removed from each well, and 130 μL of preexposure medium was added. Unless otherwise noted, the preexposure proceeded for ∼1 h before stimulation, and, because the luminometer recordings take ∼45 min to measure all of the wells, the preexposure generally lasted for 1–1.75 h. In the serial-preexposure experiment (Fig. 2*F*), the first preexposure proceeded for 1 h, and the second preexposure was done immediately before luminometry readings. Therefore, the second preexposure proceeded for ∼5–45 min before a given well was stimulated and recorded. In the time-course measurements (Fig. 2*E*), the wells were preexposed with staggered start times, factoring in the additional time required for the plate reader to reach a given well during measurement. Unless otherwise noted, the preexposure medium was water, resulting in a final diluted osmolarity of 41 mOsmol/L, with a starting medium of 21 mOsmol/L. In the potentiated responses, unless otherwise noted, the preexposure medium was 256 mM sorbitol, resulting in a final diluted osmolarity of 149 mOsmol/L with the starting medium. In the experiments involving ABA, HS-ABA, pharmacological agents, and various starting osmolarities (Fig. 4), the preexposure solutions contained 2× the final diluted concentrations of the compounds. HS-ABA was synthesized as a racemic alkyl thioether, according to methods in refs. 33 and 61. In the experiments evaluating pharmacological inhibition of osmotic-induced Ca^{2+} responses, the compounds were dissolved in the stock solvents indicated in Table S1 and then were diluted in water and the medium in the well to their final concentrations indicated in Table S1. These solutions were incubated for 30 min before stimulation. The drug concentrations used were determined from previously reported studies and our own dose–response analyses. In all cases, just before luminometry recordings, 130 μL (0.5 of the volume) of the medium was removed to allow enough empty volume for stimulation solutions.

The 96-well plates containing seedlings were loaded into a Berthold Mithras LB930 luminometer plate reader. Luminescence was measured every 0.1 s for 5 s to establish a baseline reading, and then 100 μL of stimulation solution was injected automatically at the device's highest rate to ensure the shortest disruption of recording. Unless otherwise noted, the injected stimulation solution was 700 mM sorbitol. In the dose–response measurements in Fig. 1, stimulation was done with NaCl because of the solubility limits of sorbitol. The lower-osmolarity dose dependencies were confirmed with sorbitol stimulus. After application, light was measured every 0.1 s for an additional 30 s to 1 min. Because of the mechanical limitations of the luminometer, there was generally a period of 0.2 s during application when light could not be measured. The data from these recordings were exported as tab-separated values on spreadsheets and were designated as the "stimulus-induced" luminescence data.

After all 96 wells had been stimulated and measured, the plate was removed from the luminometer, and 100 μL of solution was removed from each well. The plate was loaded into the luminometer again. Luminescence was measured every 0.1 s for 2 s to establish a baseline reading, and then 100 μL of the 2 M $CaCl_2$ + 20% ethanol solution was injected automatically at the device's highest rate to ensure the shortest disruption of recording. After application, light was measured every 0.1 s for an additional 15–30 s. The data from these recordings were exported as tab-separated values on spreadsheets and were designated as the "aequorin discharge" luminescence data.

Quantification of Response Features. A data-analysis script was written in R (62) to quantify features of individual responses as well as averages of conditions or genotypes (Dataset S1). Raw light emission was converted to Ca^{2+} concentration by the empirically determined formula pCa = 0.332588(−logk) + 5.5593, where k is a rate constant equal to stimulus-induced luminescence counts per second divided by total remaining counts (elicited by discharge by 2 M $CaCl_2$ + 20% ethanol) (25). It should be noted that this calculation assumes that all cells containing aequorin are responsive to the stimulus. Because this assumption may not always hold true, the calculated apparent $[Ca^{2+}]_i$ may underestimate the true $[Ca^{2+}]_i$. The $[Ca^{2+}]_i$s reported in this study reflect the apparent $[Ca^{2+}]_i$.

Peak detection was performed using the Peaks library (cran.r-project.org/web/packages/Peaks/index.html), using empirically established values that generally fit the observed peaks: The primary peak was defined as the first observable peak subsequent to stimulation. The secondary peak was defined as the largest detected peak that was not the primary peak. The largest peaks were normalized to a maximum value of 1 and were fit to the single exponential decay function $R = \exp(-T/\tau)$, where R is the response amplitude at time T, and τ is the decay time constant. Given that the termination kinetics were much slower than activation kinetics, a calculation of integrated area under the normalized peak also served as a useful metric of termination kinetics. Each of the calculated features was initially plotted in "beeswarm" stripcharts depicting individuals, averages, and confidence intervals (cran.r-project.org/web/packages/beeswarm/index.html) (Figs. S3 and S4), and the calculated values were used for subsequent statistical analyses.

Imaging of Whole-Seedling Ca^{2+} Responses. Ethanol-sterilized seeds were plated on medium containing 1/2 MS medium (2.2 g/L), 0.5 g/L MES, and 1.5% Phyto Agar. The plates were wrapped in Micropore tape (3M) and were cold stratified for 2–3 d at 4 °C in the dark. The plates were transferred to a growth cabinet, and the seedlings were grown vertically for 6.5 d under 16-h light/8-h dark, 22 °C, 60–80 μEm^2/s light intensity. The evening before the experiment, the vertical plate was repositioned to lie flat horizontally. A few drops of 37 °C 0.5% low-melt agarose were added along the length of the seedlings (both shoots and roots) to affix the seedlings to the plate. After the agarose solidified, 20 mL of water containing 1 μM native Ctz was added to the plate. The plate was covered in aluminum foil and placed back in the growth cabinet overnight.

The following day, the solution containing Ctz was decanted off the plate, and the plate was placed horizontally in an imaging cabinet. A CCD camera was used to image the light emitting from the seedlings. For sorbitol stimulation, 25 mL of 1-M sorbitol was dispensed onto the seedlings, and the photographs integrated light for 30 s. The sorbitol stimulation solution was decanted off the plate, and the plate was again placed horizontally in the imaging cabinet. Twenty-five milliliters of 2 M $CaCl_2$ + 20% ethanol was dispensed onto the seedlings, and the photographs integrated light for 1–2 min. The photographs were subsequently pseudocolored in ImageJ with the "Fire" lookup table to emphasize light emission intensities.

ACKNOWLEDGMENTS. We thank Antony Dodd, Zhen-Ming Pei, and Marc Knight for aequorin-expressing *Arabidopsis* seed lines and vectors; Jose Pruneda-Paz and Katia Bonaldi for support with imaging of seedlings; Felix Hauser for guidance in data analysis; Elizabeth Haswell for providing the *msl* quintuple mutant; and Hidetoshi Iida for providing the *mca1;mca2* double mutant. A.B.S. was supported by a fellowship through the Life Sciences Research Foundation, funded by the US Department of Energy, Office of Science, Office of Basic Energy Sciences, Physical Biosciences. This project was funded by NIH Grants GM060396 and ES010337 and National Science Foundation (NSF) Grant MCB-1616236 (to J.I.S.) and, in part, by NSF Career Grant IOS-1553506 (to H.-H.K.). H.-H.K. was supported by a Human Frontier Science Program Long-Term Fellowship and an Alexander von Humboldt Feodor Lynen Fellowship.

1. Hu H, Xiong L (2014) Genetic engineering and breeding of drought-resistant crops. *Annu Rev Plant Biol* 65(1):715–741.
2. Deinlein U, et al. (2014) Plant salt-tolerance mechanisms. *Trends Plant Sci* 19(6): 371–379.
3. Farooq M, Wahid A, Kobayashi N, Fujita D, Basra SMA (2009) Plant drought stress: Effects, mechanisms and management. *Sustainable Agriculture*, eds Lichtfouse E, Navarrete M, Debaeke P, Véronique S, Alberola C (Springer Netherlands, Dordrecht, The Netherlands), pp 153–188.
4. Haswell ES, Verslues PE (2015) The ongoing search for the molecular basis of plant osmosensing. *J Gen Physiol* 145(5):389–394.
5. Knight H, Trewavas AJ, Knight MR (1997) Calcium signalling in Arabidopsis thaliana responding to drought and salinity. *Plant J* 12(5):1067–1078.
6. Shimomura O, Johnson FH, Saiga Y (1962) Extraction, purification and properties of aequorin, a bioluminescent protein from the luminous hydromedusan, Aequorea. *J Cell Comp Physiol* 59(3):223–239.
7. Zhang Y, et al. (2015) Aequorin-based luminescence imaging reveals differential calcium signalling responses to salt and reactive oxygen species in rice roots. *J Exp Bot* 66(9):2535–2545.
8. Saidi Y, et al. (2009) The heat shock response in moss plants is regulated by specific calcium-permeable channels in the plasma membrane. *Plant Cell* 21(9):2829–2843.
9. Tracy FE, Gilliham M, Dodd AN, Webb AAR, Tester M (2008) NaCl-induced changes in cytosolic free Ca2+ in Arabidopsis thaliana are heterogeneous and modified by external ionic composition. *Plant Cell Environ* 31(8):1063–1073.
10. Munns R, Tester M (2008) Mechanisms of salinity tolerance. *Annu Rev Plant Biol* 59(1): 651–681.
11. Schmöckel SM, et al. (2015) Different NaCl-induced calcium signatures in the Arabidopsis thaliana ecotypes Col-0 and C24. *PLoS One* 10(2):e0117564.
12. Choi W-G, Toyota M, Kim S-H, Hilleary R, Gilroy S (2014) Salt stress-induced Ca2+ waves are associated with rapid, long-distance root-to-shoot signaling in plants. *Proc Natl Acad Sci USA* 111(17):6497–6502.

13. Xiong TC, et al. (2014) Imaging long distance propagating calcium signals in intact plant leaves with the BRET-based GFP-aequorin reporter. *Front Plant Sci* 5:43.
14. Zhu X, Feng Y, Liang G, Liu N, Zhu J-K (2013) Aequorin-based luminescence imaging reveals stimulus- and tissue-specific Ca2+ dynamics in Arabidopsis plants. *Mol Plant* 6(2):444–455.
15. Yuan F, et al. (2014) OSCA1 mediates osmotic-stress-evoked Ca2+ increases vital for osmosensing in Arabidopsis. *Nature* 514(7522):367–371.
16. Choi J, et al. (2014) Identification of a plant receptor for extracellular ATP. *Science* 343(6168):290–294.
17. Haruta M, Sabat G, Stecker K, Minkoff BB, Sussman MR (2014) A peptide hormone and its receptor protein kinase regulate plant cell expansion. *Science* 343(6169): 408–411.
18. Hou C, et al. (2014) DUF221 proteins are a family of osmosensitive calcium-permeable cation channels conserved across eukaryotes. *Cell Res* 24(5):632–635.
19. Kramer PJ, Boyer JS (1995) *Water Relations of Plants and Soils* (Academic, Cambridge, MA).
20. Nomura H, Komori T, Kobori M, Nakahira Y, Shiina T (2008) Evidence for chloroplast control of external Ca2+-induced cytosolic Ca2+ transients and stomatal closure. *Plant J* 53(6):988–998.
21. Nomura H, Shiina T (2014) Calcium signaling in plant endosymbiotic organelles: Mechanism and role in physiology. *Mol Plant* 7(7):1094–1104.
22. Shih H-W, Miller ND, Dai C, Spalding EP, Monshausen GB (2014) The receptor-like kinase FERONIA is required for mechanical signal transduction in Arabidopsis seedlings. *Curr Biol* 24(16):1887–1892.
23. Monshausen GB, Haswell ES (2013) A force of nature: Molecular mechanisms of mechanoperception in plants. *J Exp Bot* 64(15):4663–4680.
24. Martí MC, Stancombe MA, Webb AAR (2013) Cell- and stimulus type-specific intracellular free Ca2+ signals in Arabidopsis. *Plant Physiol* 163(2):625–634.
25. Knight H, Trewavas AJ, Knight MR (1996) Cold calcium signaling in Arabidopsis involves two cellular pools and a change in calcium signature after acclimation. *Plant Cell* 8(3):489–503.
26. Lisman J, Yasuda R, Raghavachari S (2012) Mechanisms of CaMKII action in long-term potentiation. *Nat Rev Neurosci* 13(3):169–182.
27. Veldstra H (1956) Synergism and potentiation with special reference to the combination of structural analogues. *Pharmacol Rev* 8(3):339–387.
28. Kiegle E, Moore CA, Haseloff J, Tester MA, Knight MR (2000) Cell-type-specific calcium responses to drought, salt and cold in the Arabidopsis root. *Plant J* 23(2):267–278.
29. Zeevaart JAD, Creelman RA (1988) Metabolism and physiology of abscisic acid. *Annu Rev Plant Physiol Plant Mol Biol* 39(1):439–473.
30. Verslues PE, Agarwal M, Katiyar-Agarwal S, Zhu J, Zhu J-K (2006) Methods and concepts in quantifying resistance to drought, salt and freezing, abiotic stresses that affect plant water status. *Plant J* 45(4):523–539.
31. Hauser F, Waadt R, Schroeder JI (2011) Evolution of abscisic acid synthesis and signaling mechanisms. *Curr Biol* 21(9):R346–R355.
32. Brady SM, et al. (2015) Reassess the t test: Interact with all your data via ANOVA. *Plant Cell* 27(8):2088–2094.
33. Takeuchi J, et al. (2014) Designed abscisic acid analogs as antagonists of PYL-PP2C receptor interactions. *Nat Chem Biol* 10(6):477–482.
34. Nakagawa Y, et al. (2007) Arabidopsis plasma membrane protein crucial for Ca2+ influx and touch sensing in roots. *Proc Natl Acad Sci USA* 104(9):3639–3644.
35. Yamanaka T, et al. (2010) MCA1 and MCA2 that mediate Ca2+ uptake have distinct and overlapping roles in Arabidopsis. *Plant Physiol* 152(3):1284–1296.
36. Wilson ME, Maksaev G, Haswell ES (2013) MscS-like mechanosensitive channels in plants and microbes. *Biochemistry* 52(34):5708–5722.
37. Hanikenne M, Bernal M, Urzica E-I (2014) Ion homeostasis in the chloroplast. Plastid biology. *Advances in Plant Biology*, eds Theg SM, Wollman F-A (Springer, New York), pp 465–514.
38. Stael S, et al. (2012) Plant organellar calcium signalling: An emerging field. *J Exp Bot* 63(4):1525–1542.
39. Aranda-Sicilia MN, et al. (2012) Arabidopsis KEA2, a homolog of bacterial KefC, encodes a K(+)/H(+) antiporter with a chloroplast transit peptide. *Biochim Biophys Acta* 1818(9):2362–2371.
40. Sze H, et al. (2004) Expression patterns of a novel AtCHX gene family highlight potential roles in osmotic adjustment and K+ homeostasis in pollen development. *Plant Physiol* 136(1):2532–2547.
41. Kunz H-H, et al. (2014) Plastidial transporters KEA1, -2, and -3 are essential for chloroplast osmoregulation, integrity, and pH regulation in Arabidopsis. *Proc Natl Acad Sci USA* 111(20):7480–7485.
42. Armbruster U, et al. (2014) Ion antiport accelerates photosynthetic acclimation in fluctuating light environments. *Nat Commun* 5:5439.
43. Sani E, Herzyk P, Perrella G, Colot V, Amtmann A (2013) Hyperosmotic priming of Arabidopsis seedlings establishes a long-term somatic memory accompanied by specific changes of the epigenome. *Genome Biol* 14(6):R59.
44. Virlouvet L, Fromm M (2015) Physiological and transcriptional memory in guard cells during repetitive dehydration stress. *New Phytol* 205(2):596–607.
45. Ding Y, Fromm M, Avramova Z (2012) Multiple exposures to drought 'train' transcriptional responses in Arabidopsis. *Nat Commun* 3:740.
46. Takahashi Y, Kinoshita T (2015) Stomatal function has an element of hysteresis. *New Phytol* 205(2):455–457.
47. Spalding EP, Harper JF (2011) The ins and outs of cellular Ca(2+) transport. *Curr Opin Plant Biol* 14(6):715–720.
48. Alon U, Surette MG, Barkai N, Leibler S (1999) Robustness in bacterial chemotaxis. *Nature* 397(6715):168–171.
49. Muzzey D, Gómez-Uribe CA, Mettetal JT, van Oudenaarden A (2009) A systems-level analysis of perfect adaptation in yeast osmoregulation. *Cell* 138(1):160–171.
50. Yi T-M, Huang Y, Simon MI, Doyle J (2000) Robust perfect adaptation in bacterial chemotaxis through integral feedback control. *Proc Natl Acad Sci USA* 97(9): 4649–4653.
51. Waadt R, et al. (2014) FRET-based reporters for the direct visualization of abscisic acid concentration changes and distribution in Arabidopsis. *eLife* 3:e01739.
52. Finazzi G, et al. (2015) Ions channels/transporters and chloroplast regulation. *Cell Calcium* 58(1):86–97.
53. Rizzuto R, De Stefani D, Raffaello A, Mammucari C (2012) Mitochondria as sensors and regulators of calcium signalling. *Nat Rev Mol Cell Biol* 13(9):566–578.
54. Pozzan T, Rizzuto R, Volpe P, Meldolesi J (1994) Molecular and cellular physiology of intracellular calcium stores. *Physiol Rev* 74(3):595–636.
55. Han L, Li JL, Wang L, Shi WM, Su YH (2015) Identification and localized expression of putative K+/H+ antiporter genes in Arabidopsis. *Acta Physiol Plant* 37(5):1–14.
56. Jarvis P, López-Juez E (2013) Biogenesis and homeostasis of chloroplasts and other plastids. *Nat Rev Mol Cell Biol* 14(12):787–802.
57. Ytterberg AJ, Peltier J-B, van Wijk KJ (2006) Protein profiling of plastoglobules in chloroplasts and chromoplasts. A surprising site for differential accumulation of metabolic enzymes. *Plant Physiol* 140(3):984–997.
58. Loro G, et al. (2016) Chloroplast-specific in vivo Ca2+ imaging using Yellow Cameleon fluorescent protein sensors reveals organelle-autonomous Ca2+ signatures in the stroma. *Plant Physiol* 171(4):2317–2330.
59. Wilson ME, Basu MR, Bhaskara GB, Verslues PE, Haswell E (2014) Plastid osmotic stress activates cellular stress responses in Arabidopsis thaliana. *Plant Physiol* 165(1): 119–128.
60. Knight MR, Campbell AK, Smith SM, Trewavas AJ (1991) Transgenic plant aequorin reports the effects of touch and cold-shock and elicitors on cytoplasmic calcium. *Nature* 352(6335):524–526.
61. Todoroki Y, Hirai N, Ohigashi H (1995) Synthesis, biological activity and metabolism of (S)-(+)-3′-Fluoroabscisic acid. *Tetrahedron* 51(25):6911–6926.
62. R Core Team (2013) *R: A Language and Environment for Statistical Computing* (R Foundation for Statistical Computing, Vienna).